RESEARCH ARTICLE | MAY 15 2023

The torsion pendulum dual oscillator for low-frequency Newtonian noise detection

Special Collection: Gravitational Wave Detectors

S. S. Y. Chua [®] ; N. A. Holland [®] ; P. W. F. Forsyth [®] ; A. Kulur Ramamohan [®] ; Y. Zhang [®] ; J. Wright [®] ; D. A. Shaddock [®] ; D. E. McClelland [®] ; B. J. J. Slagmolen ■ [®]

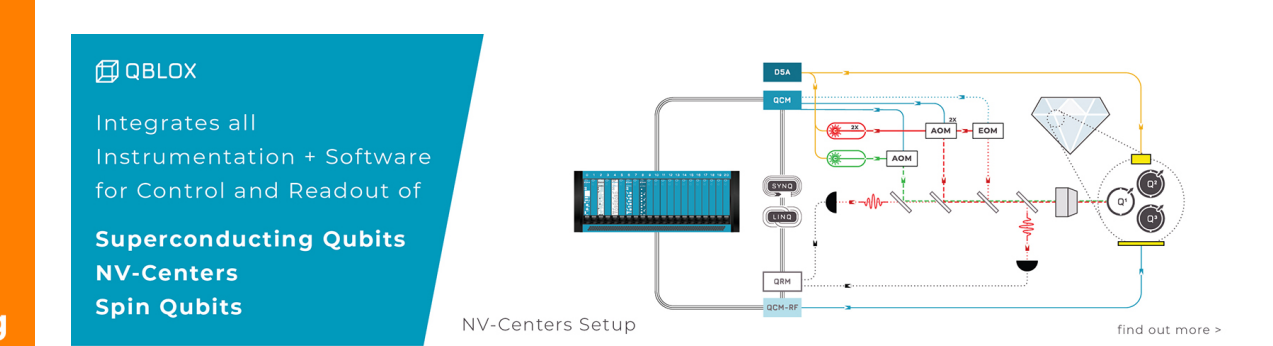


Appl. Phys. Lett. 122, 201102 (2023) https://doi.org/10.1063/5.0145092





CrossMark





The torsion pendulum dual oscillator for low-frequency Newtonian noise detection

Cite as: Appl. Phys. Lett. **122**, 201102 (2023); doi: 10.1063/5.0145092 Submitted: 2 February 2023 · Accepted: 27 April 2023 · Published Online: 15 May 2023







AFFILIATIONS

OzGrav-ANU, Center for Gravitational Astrophysics, Research Schools of Physics, and of Astronomy and Astrophysics, The Australian National University, Canberra ACT 2601, Australia

Note: This paper is part of the APL Special Collection on Gravitational Wave Detectors.

^{a)}Present address: Dutch National Institute for Subatomic Physics, Nikhef, 1098 XG Amsterdam, The Netherlands and Vrije Universiteit Amsterdam, 1081 HV Amsterdam, The Netherlands.

ABSTRACT

We present a torsion pendulum dual oscillator sensor designed toward the direct detection of Newtonian noise. We discuss the sensitivity limitations of the system, experimental performance characterization results, and prospectives to improve performance. The sensor is being developed to contribute to the mitigation of Newtonian noise impacts in the sensitivities of next generation terrestrial gravitational-wave detectors.

© 2023 Author(s). All article content, except where otherwise noted, is licensed under a Creative Commons Attribution (CC BY) license (http://creativecommons.org/licenses/by/4.0/). https://doi.org/10.1063/5.0145092

The terrestrial laser interferometric gravitational-wave detectors represent the most sensitive displacement sensors to date. ^{1–3} These devices are able to register gravitational waves from massive accelerating astronomical objects, ⁴ and have detected an array of signals such as mergers of binary black holes ^{5,6} and binary neutron stars. ⁷ The next generation of instruments ^{8,9} seek to build on the experiences and expertise of the current detectors to significantly improve the sensitivity of the detector network.

Newtonian noise (NN), also known as gravity gradient noise, ¹⁰ is a potential limiting noise source for these future detectors at frequencies below 20 Hz. ¹¹ NN is caused by shifts in the local density profile of matter around a gravitational-wave detector, which gives rise to gravitational field fluctuations that induce time-dependent net forces on the test mass mirrors of the detector. ¹² Gravitational-wave detectors cannot be *a priori* shielded from NN, especially in the horizontal plane of greatest interest to the interferometers. ^{10,11,13} The ability to quantify NN by modeling of potential sources is often complicated, as any particular local environment may have a high diversity of NN sources, such as seismic, atmospheric, hydrological, or anthropogenic sources. ¹⁴ As such, a direct NN sensor that is deployable within the local environment of a gravitational-wave detector would be invaluable. A direct measure would allow the NN contributions to be signal-processed from the gravitational-wave detector's readout. ¹⁵

A global research effort to develop methods and sensors to continuously measure gravitational field fluctuations for mitigating NN is under way. ^{16–18} A diverse array of detectors of assorted sizes and geometries have been developed, from compact micro-electromechanical system gravimeters ¹⁹ to mid-scale torsion pendulum designs. ^{20,21} In this paper, we present one of these mid-scale torsion pendulum detectors—the torsion pendulum dual oscillator (TorPeDO). After an overview of the mechanical design and the mechanical response to NN, we present the optical readout of the sensor and discuss the sensitivity limits of the system. We then present performance characterization results of the sensor. We finally present prospectives for the sensor—active lines of research pursuing radically improved performance.

The torsion pendulum dual oscillator (TorPeDO) consists of two torsion pendulums, as shown in Fig. 1. The two pendulums are suspended in a cross formation, with a vertical space of 10 mm between the horizontal bars at the center of the cross. Each torsion pendulum is a $\sim\!850$ mm long dumbbell-like beam. The centers of mass of the pendulums are designed to overlap at the midpoint of the vertical space, 5 mm above (below) the lower (upper) pendulum horizontal bar. Each pendulum is suspended with two 600 mm long, 431.8 μm diameter, tungsten suspension wires that are attached to each pendulum at a height of $\sim\!85$ mm above their centers of mass. NN induces a time-dependent net force across the end masses of a pendulum and, thus,

b) Author to whom correspondence should be addressed: bram.slagmolen@anu.edu.au

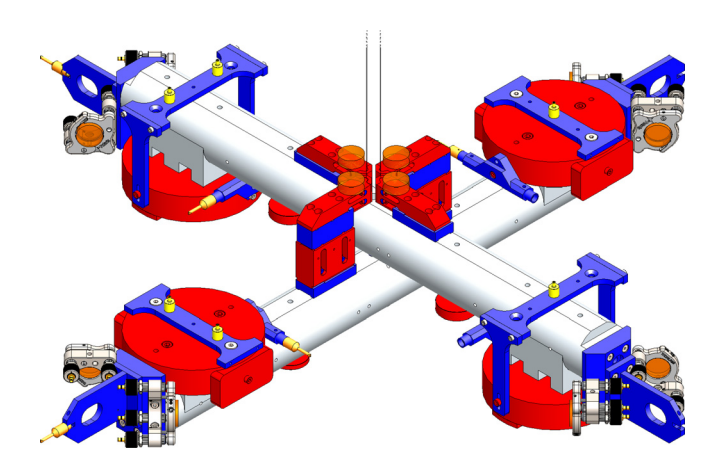


FIG. 1. CAD rendering of the TorPeDO sensor, with the two pendulum beams.

will generate a time-dependent torque on each pendulum. This results in a differential torque, with a time-dependent differential rotation angle, between the two pendulums. Therefore, by interrogating the differential rotation angle, the TorPeDO can directly measure the NN effects without relying on additional knowledge for the measurement, such as accurate parameters of local topography or geology.^{22–24}

Furthermore, torsion pendula systems have a key advantage of being able to be designed with mechanical resonances at low Fourier frequencies 20 suitable for NN measurement. For the TorPeDO, the pendulums have a torsional mechanical resonance frequency of $\sim \!\! 26$ mHz. Above the torsional mechanical resonance frequency, the pendulums act as rigid bodies in effective free fall. Key parameters are listed in Table I.

The TorPeDO geometry has limits in responsivity to certain NN directional components, for example, it is insensitive to vertical NN components. However, the largest component of the directional responsivity is the horizontal quadrapole moment. This coincides with the NN effects on the horizontal plane, the direction of greatest interest to gravitational-wave detectors.

TABLE I. TorPeDO pendulum parameters and resonant mode frequencies.

Parameter	Beam 1	Beam 2
Mass (kg)	14.65	13.65
Wire length (mm)—two per pendulum	600	600
Wire diameter (μ m)	431.8	431.8
Yaw (Hz)	0.0268	0.0262
Longitudinal (Hz)	0.6016	0.6147
Transverse (Hz)	0.6141	0.6015
Pitch (Hz)	1.0334	3.5606
Roll (Hz)	3.8299	1.0255
Vertical (Hz)	18.6335	19.1080
Roll moment of inertia I_{xx} (kg m ²)	0.0248	0.7469
Pitch moment of inertia I_{yy} (kg m ²)	0.7530	0.0273
Yaw moment of inertia I_{zz} (kg m ²)	0.7504	0.7503

The optical setup for measuring the differential rotation between the two pendulums is shown in Fig. 2. Four Fabry–Pérot optical cavities are constructed, with their partially reflecting mirrors placed upon the ends of each beam. Differential rotation of the pendulums causes common expansion and contraction of geometrically opposite cavities. Interrogating an appropriate combination of cavity length changes gives the rotation angle readout of the sensor.

Each of the four cavities are interrogated using the Pound–Drever–Hall (PDH) locking method, 25,26 with their own individual laser and PDH optical path, as shown in Fig. 2. The PDH error signal is fed back to the laser to maintain cavity resonance. The PDH error signal also encodes the cavity length change, and is used to reconstruct the differential rotation angle of the two pendulums. With a cavity finesse of ~ 150 and incident laser power of 10 mW, the displacement equivalent shot noise is 4×10^{-18} m/ $\sqrt{\rm Hz}$. With a 24 cm mechanical lever arm, this sets an equivalent differential angular limit due to shot noise of 10^{-17} rad/ $\sqrt{\rm Hz}$.

Although the dominant cavity length change is caused by the differential rotation of the pendulums, any other differential pendulum motion will be registered by the optical cavities. For example, the longitudinal motion of one pendulum relative to the transverse motion of the second pendulum will also change the respective cavity lengths. Alternative combinations of cavity length changes witness these lateral motions. With each pendulum having six degrees of freedom, the sensing and control matrices are carefully measured to minimize the sensing and actuation coupling of the other modes into the differential rotation.

The pendulums are configured with local sensors and actuators (BOSEMs and AOSEMs²⁷), which can be used for local readout and local suspension damping. Use of the local sensors and actuators is dependent on the residual motion of the torsion pendulums and their control configuration, as their effective sensor noise will be reinjected via the local actuators. Hence, these actuators are only used during system lock acquisition and times of high residual motion.

As previously stated, the TorPeDO sensor pendulums experience a net torque from local NN, and thus the sensor response can be expressed in terms of differential torque between the two pendulums. Being a suspended system, the suspension thermal noise, a consequence of the fluctuation-dissipation theorem and structural losses in mechanical systems, ²⁸ sets a lower bound for the differential torque sensitivity. In the TorPeDO, structural losses are dominated by the energy lost in the twisting and deformation of the suspension wires. Using the parameters from Table I, the estimated suspension-thermal-noise-limited differential torque spectrum is shown in Fig. 3.

The target sensitivity of the TorPeDO is to reach the residual motion driven by fundamental noise mechanisms, namely, the suspension thermal noise of the TorPeDO mechanics and the shot noise of the optical readout.

The suspension thermal noise limit is derived from the differential torque spectrum, as shown in Fig. 3, through conversion to differential angle units. The torque-to-angle transfer function H_{τ} for a single torsion pendulum system is given by

$$H_{\tau,i} = \frac{\theta}{\tau} = \frac{1}{I_i \sqrt{(\omega_{0,i}^2 - \omega^2)^2 + (\omega_{0,i}^2/Q)^2}},$$
 (1)

where $\omega_{0,i} = 2\pi f_{0,i}$ and $f_{0,i}$ is the yaw resonance frequency in Hz of the *i*-th pendulum, I_i is the yaw moment of inertia in kg m², and Q is

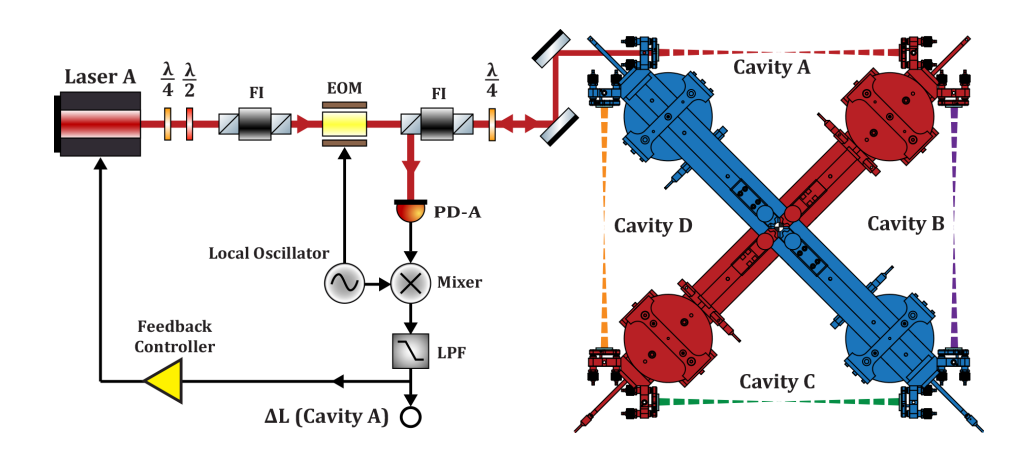


FIG. 2. Optical readout of the TorPeDO sensor. Four optical cavities are formed between the torsion pendulums. Each cavity length change is interrogated using an independent laser and the Pound–Drever–Hall system (Cavity A system only shown for clarity). FI—Faraday isolator, $\lambda/2$ —half-wave plate, $\lambda/4$ —quarter wave plate, LPF—low pass filter, PD—photodetector, EOM—electro-optic modulator.

the tungsten wire quality factor of 10^6 . The *i* denotes the parameters of pendulum 1 or 2, with the total transfer function being the summation of the two transfer functions ($H_{tot} = H_{\tau,1} + H_{\tau,2}$). Once converted, the suspension thermal noise limit is quadrature-summed with the shot noise differential angular limit level to form the total angular sensitivity.

Figure 4 shows the modeled performance of the TorPeDO sensor, in terms of differential angle between the two pendulums. The sensor's total sensitivity, curve (a), has a Fourier frequency band of interest from 10 mHz to 10 Hz, and is limited by the tungsten suspension wire thermal noise (b) up to 5 Hz. Above 5 Hz, shot noise from the cavity readout scheme (c) forms the dominant sensor limitation.

No external damping is applied to the resonances within the model, so as to prevent contaminating the TorPeDO's performance with local sensor and actuator noises. Furthermore, the modeling includes a mismatch of centers of mass of 566 μ m to mimic tolerances from machining and assembly of the physical TorPeDO system. However, the physical system includes adjustors that allow tuning of the torsional resonance frequencies to be identical. This includes

adjustors as described in McManus *et al.*²⁹ that can allow tuning of the centers of mass positions of the pendulums to sub-200 μ m precision.

Figure 4 shows results for modeled signal levels of the dominant NN sources of interest for terrestrial gravitational-wave detectors projected onto the differential angle sensor basis. These sources are infrasound NN, ocurve (d), and NN from seismic Rayleigh (e) and body waves (f) based from Streckeisen STS-2 seismometer readings of the local ground motion of our laboratory. Each type of NN driver is predicted to be at least an order of magnitude larger than the TorPeDO sensitivity limit curve for a significant part of the TorPeDO sensor's Fourier band of interest—below 600 mHz will be the region with the greatest predicted separation.

To verify the TorPeDO sensor sensitivity, an external calibration tone with known gravitational field parameters can be applied. These types of calibrations, from Newtonian Calibrator devices, have been used in the terrestrial gravitational-wave detectors. ^{32,33} Point (g) in Fig. 4 is a modeled tone based on simulation ³⁴ with an existing nominal calibration device design. This highlights a method of TorPeDO sensor verification independent of background NN effect strength.

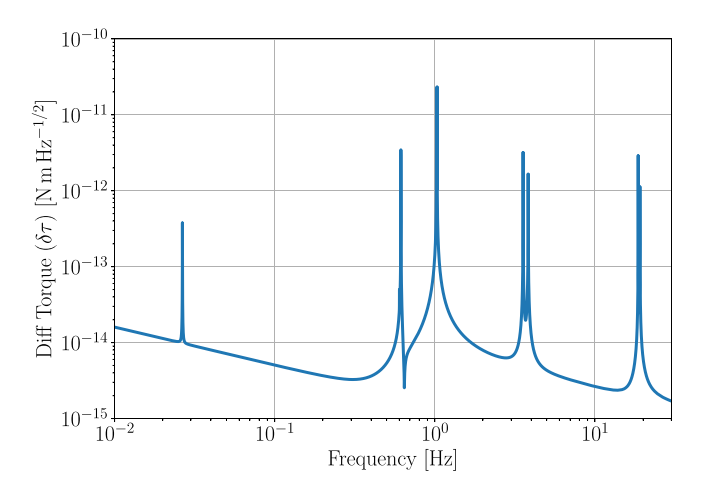


FIG. 3. The modeled suspension-thermal-noise-limited differential torque spectrum of the TorPeDO sensor. From left to right, the resonances are the yaw, longitudinal, transverse, pitch, roll, and vertical modes of the two pendulums.

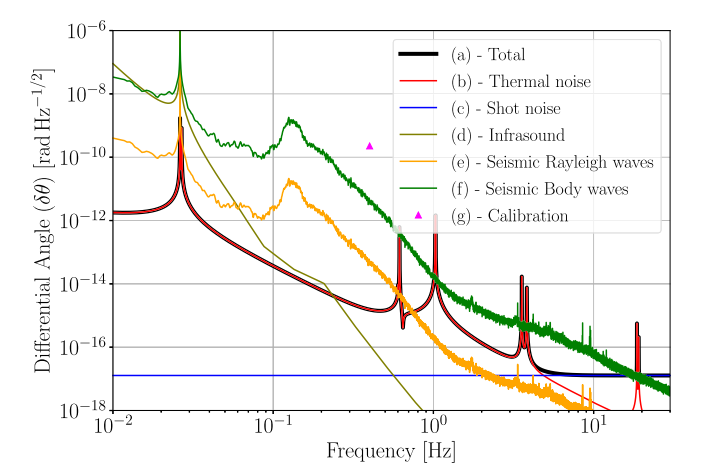


FIG. 4. Projected TorPeDO differential rotation angle sensitivity limits and Newtonian noise models. The total noise, curve (a), is the quadrature sum of the thermal noise (b) and shot noise (c) contributions. Curves (d)–(f) project noise strengths of different NN sources. Point (g) is a nominal calibration tone, discussed in the text.

The TorPeDO sensor has been operated in a control prototype measurement run. ³⁵ During this run, the suspension point was rigidly attached to the ground. Repeatable autonomous operation was achieved using the PDH locking scheme shown in Fig. 2, and the BOSEM and AOSEM local sensors as independent witnesses. The controls prototype was operated in air and represents an upper performance limit for the TorPeDO.

Figure 5 shows the calibrated differential rotation signal measurement. The 4×1 linear matrix combination of the cavity length changes, extracted from the cavities' PDH readout, is labelled "DRZ" and shown by curve (A), where the suppression provided by the PDH control loops have been compensated. Measurements are transformed from the cavity basis to differential rotation angle by a measured, frequency-independent matrix.

Local sensor measurements of each pendulum are propagated to the equivalent differential-angle basis using measured transfer functions. Curve (B) represents the yaw or rotational degree-of-freedom, curve (C), the longitudinal and transverse degrees-of-freedom, and curve (D), the remaining pitch, roll, and vertical degrees-of-freedom, local sensor measurements. Curve (E) represents a quadrature-sum estimate of freerunning laser frequency noise of the independent PDH lasers.

Below 90 mHz, the differential rotation is consistent with the differential rotation observed by the local sensors. Differential rotation, observed by either cavity DRZ or local sensor system, is the dominant motion at these frequencies. The roll-off in the local sensor yaw signal (B) above 100 mHz is due to artificial attenuation from elliptic cutoff filters. Between 200 and 600 mHz, imperfect subtraction of the longitudinal and transverse motion occurs in the PDH readout. This imperfect subtraction can be improved with a coherent subtraction of the motion as witnessed through non-DRZ combinations of the PDH readout signals, or with a frequency-dependent matrix based on the same data used to generate the frequency-independent matrix.

Above 600 mHz, the signal is consistent with residual coupling from the other pendulum degrees-of-freedom. This motion does not necessarily linearly couple into the cavity sensing basis. Comparison between the cavity and local sensor signals shows up to an order of magnitude cancelation of the pitch and roll modes in the cavity signal,

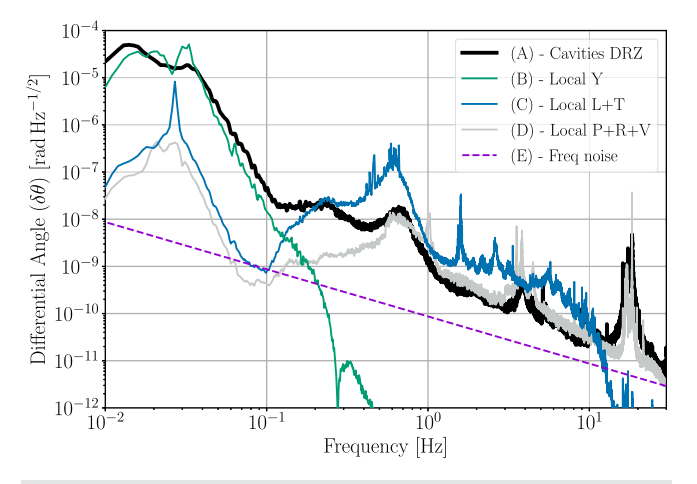


FIG. 5. TorPeDO sensor prototype performance. (A) PDH readout from the cavities, (B)–(D) local sensor measurement of the degrees of freedom, and (E) estimated laser frequency noise.

while the vertical modes, present at higher frequencies, do not impact the low-frequency measurement.

At all frequencies, the differential motion measured by the PDH system is consistent with the sensor displacement observed from the local sensors.

To extend the controls prototype performance toward reaching the equivalent thermal noise and shot noise limit of the TorPeDO sensor, a number of upgrades are being commissioned.

First, operation of the controls prototype has noted an increase in differential yaw motion with increased airflow across the experiment. Placing the system in high vacuum will mitigate air currents, air temperature gradients, and other acoustic environmental influences in the readout

Second, to mitigate direct large-scale seismic coupling to the sensor, the suspension point of the TorPeDO pendulums will no longer have rigid connection to the ground. Instead, the TorPeDO will be suspended from a seismic isolation chain.³⁶ A mechanical CAD rendering of the seismic isolation chain and TorPeDO sensor is shown in Fig. 6. The isolation chain starts with a MultiSAS³⁷ isolation system for first-stage attenuation against direct seismic ground motion. Additional inertia sensors (three Nanometrics Trillium 240 seismometers³⁸) measure residual motion after this first attenuation stage and are used in a feedback loop to reduce the MultiSAS horizontal motion down to their measurement noise floor. Next are a suspended

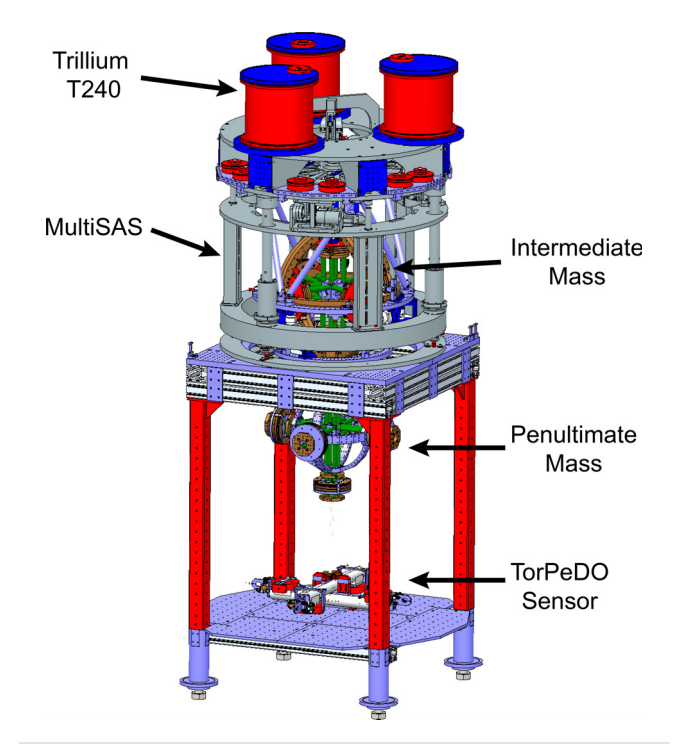


FIG. 6. CAD rendering of the TorPeDO seismic isolation chain with the TorPeDO Sensor. The cylindrical MultiSAS system is rested on the square support frame, with three vacuum cans housing the three Trillium 240 seismometers. The spherical intermediate mass is suspended from the MultiSAS as the second stage, followed by the penultimate mass stage. The TorPeDO pendulums form the sensor at the final stage. The entire seismic isolation chain and TorPeDO system will be housed in a high-vacuum system (not shown).

 $140.66\,kg$ intermediate mass stage, and then a 53.19 kg penultimate mass stage. Each mass stage has local sensors and actuators, referenced to the previous mass stage in the chain. The seismic isolation chain will provide a suspension point for the TorPeDO pendulums with residual displacement motion of $1.9\times10^{-10}\,m/\sqrt{Hz}$ and residual rotation motion of $3.9\times10^{-12}\,rad/\sqrt{Hz}$ at 0.1 Hz frequency, which should facilitate the TorPeDO sensor to be at the level of its suspension-thermal-noise-limited sensitivity. 36

The substantial reduction in input motion provided by these two upgrades will remove the necessity to use the local sensors for damping during low-noise science operation. This supports our analysis discussed earlier, neglecting external damping of the TorPeDO sensor resonances.

Finally, as discussed for Fig. 5 curve (E), free-running laser frequency noise of the independent PDH lasers will be a technical limiting source in the cavity readout. Laser frequency noise can be mitigated by phase locking each of the four lasers to a fifth reference laser, making the noise common between the optical readouts and allowing a large common mode rejection of the frequency noise. The phase lock loops and the PDH error signals will be combined to form a cascaded hierarchical feedback to the individual laser frequency actuators.

The torsion pendulum dual oscillator (TorPeDO) has demonstrated differential rotation measurement performance at mHz Fourier frequencies where Newtonian noise effects are of primary interest. With prospective improvements, the TorPeDO sensor will become an important diagnostic tool for measuring Newtonian noise impacts in next generation gravitational-wave detectors.

This research was supported by the Australian Research Council under the ARC Centre of Excellence for Gravitational Wave Discovery, Grant No. CE170100004, Future Fellowship, Grant No. FT130100329 and Discovery Project, Grant No. DP160100760. This work has been assigned LIGO Document No. LIGO-P2300027. The authors thank D. Hickey and T. Wu for their contributions to the project.

AUTHOR DECLARATIONS Conflict of Interest

The authors have no conflicts to disclose.

Author Contributions

Sheon S. Y. Chua: Data curation (supporting); Formal analysis (supporting); Supervision (supporting); Writing – original draft (lead); Writing – review & editing (lead). Nathan A. Holland: Data curation (equal); Formal analysis (equal); Investigation (equal); Methodology (equal); Writing – original draft (equal); Writing – review & editing (equal). Perry W. F. Forsyth: Data curation (equal); Formal analysis (equal); Methodology (equal); Writing – review & editing (equal). Avanish Kulur Ramamohan: Writing – review & editing (equal). Ya Zhang: Writing – review & editing (equal). Jennifer Wright: Writing – review & editing (equal). Daniel A. Shaddock: Conceptualization (equal); Funding acquisition (equal); Supervision (supporting). David E. McClelland: Funding acquisition (lead); Data curation (equal); Formal analysis (equal); Funding acquisition

(equal); Supervision (lead); Writing – original draft (equal); Writing – review & editing (equal).

DATA AVAILABILITY

The data that support the findings of this study are available from the corresponding author upon reasonable request.

REFERENCES

- ¹J. Aasi, B. P. Abbott, R. Abbott *et al.*, "Advanced LIGO," Classical Quantum Gravity **32**, 074001 (2015).
- ²F. Acernese, M. Agathos, K. Agatsuma *et al.*, "Advanced Virgo: A second-generation interferometric gravitational wave detector," Classical Quantum Gravity **32**, 024001 (2015).
- T. Akutsu, M. Ando, K. Arai et al., "KAGRA: 2.5 generation interferometric gravitational wave detector," Nat. Astron. 3, 35 (2019).
 LIGO Collaboration, Virgo Collaboration, and KAGRA Collaboration,
- ⁴LIGO Collaboration, Virgo Collaboration, and KAGRA Collaboration, "GWTC-3: Compact binary coalescences observed by LIGO and Virgo during the second part of the third observing run," arXiv:2111.03606 (2021).
- ⁵B. P. Abbott, R. Abbott, T. D. Abbott *et al.*, "Observation of gravitational waves from a binary black hole merger," Phys. Rev. Lett. **116**, 061102 (2016).
- ⁶R. Abbott, T. D. Abbott, S. Abraham *et al.*, "GW190521: A binary black hole merger with a total mass of 150 M_{\odot} ," Phys. Rev. Lett. **125**, 101102 (2020)
- ⁷B. P. Abbott, R. Abbott, T. D. Abbott et al., "Gravitational waves and gammarays from a binary neutron star merger: GW170817 and GRB 170817A," Astrophys. J. 848(2), L13 (2017).
- ⁸M. Punturo, M. Abernathy, F. Acernese *et al.*, "The Einstein telescope: A third-generation gravitational wave observatory," Classical Quantum Gravity 19, 194002 (2010).
- ⁹E. D. Hall, K. Kuns, J. R. Smith *et al.*, "Gravitational-wave physics with cosmic explorer: Limits to low-frequency sensitivity," Phys. Rev. D **103**, 122004 (2021).
- 10 S. A. Hughes and K. S. Thorne, "Seismic gravity-gradient noise in interferometric gravitational-wave detectors," Phys. Rev. D 58, 122002 (1998).
- ¹¹M. G. Beker, J. F. J. van den Brand, E. Hennes *et al.*, "Newtonian noise and ambient ground motion for gravitational wave detectors," J. Phys.: Conf. Ser. 363, 012004 (2012).
- ¹²P. R. Saulson, "Terrestrial gravitational noise on a gravitational wave antenna," Phys. Rev. D 30, 732 (1984).
- ¹³M. Beccaria, M. Bernardini, S. Braccini *et al.*, "Relevance of Newtonian seismic noise for the Virgo interferometer sensitivity," Classical Quantum Gravity 15, 3339–3362 (1998).
- ¹⁴J. Harms, "Terrestrial gravity fluctuations," Living Rev. Relativ. **22**, 6 (2019).
- 15J. Harms and H. Paik, "Newtonian-noise cancellation in full-tensor gravitational-wave detectors," Phys. Rev. D 92, 022001 (2015).
- ¹⁶J. C. Driggers, J. Harms, and R. X. Adhikari, "Subtraction of Newtonian noise using optimized sensor arrays," Phys. Rev. D 86, 102001 (2012).
- 17J. Harms, B. J. J. Slagmolen, R. X. Adhikari et al., "Low-frequency terrestrial gravitational years detectors," Phys. Pey. D 88, 122033 (2013)
- gravitational-wave detectors," Phys. Rev. D **88**, 122033 (2013).

 18 J. Harms, E. L. Bonilla, M. W. Coughlin *et al.*, "Observation of a potential future sensitivity limitation from ground motion at LIGO Hanford," Phys. Rev. D **101**, 102002 (2020).
- ¹⁹R. P. Middlemiss, A. Samarelli, D. J. Paul *et al.*, "Measurement of the Earth tides with a MEMS gravimeter," Nature 531, 614 (2016).
- ²⁰M. Ando, K. Ishidoshiro, K. Yamamoto et al., "Torsion-bar antenna for low-frequency gravitational-wave observations," Phys. Rev. Lett. 105, 161101 (2010).
- ²¹M. P. Ross, K. Venkateswara, C. A. Hagedorn *et al.*, "A low-frequency torsion pendulum with interferometric readout," Rev. Sci. Instrum. **92**(5), 054502 (2021).
- (2021).

 22 A. Singha, S. Hild, J. Harms, M. C. Tringali *et al.*, "Characterization of the seismic field at Virgo and improved estimates of Newtonian-noise suppression by recesses," Classical Quantum Gravity 38, 245007 (2021).
- ²³M. Coughlin, N. Mukund, J. Harms et al., "Towards a first design of a Newtonian-noise cancellation system for advanced LIGO," Classical Quantum Gravity 33, 244001 (2016).

- ²⁴M. C. Tringali, T. Bulik, J. Harms *et al.*, "Seismic array measurements at Virgo's west end building for the configuration of a Newtonian-noise cancellation system," Classical Quantum Gravity 37, 025005 (2020).
- ²⁵R. W. P. Drever, J. L. Hall, F. V. Kowalski *et al.*, "Laser phase and frequency stabilization using an optical resonator," Appl. Phys. B 31, 97 (1983).
- ²⁶E. D. Black, "An introduction to Pound-Drever-Hall laser frequency stabilization," Am. J. Phys. 69(1), 79 (2001).
- ²⁷L. Carbone, S. M. Aston, R. M. Cutler *et al.*, "Sensors and actuators for the Advanced LIGO mirror suspensions," Classical Quantum Gravity 29, 115005 (2012).
- ²⁸P. R. Saulson, "Thermal noise in mechanical experiments," Phys. Rev. D 42, 2437–2445 (1990).
- ²⁹D. J. McManus, P. W. F. Forsyth, M. J. Yap et al., "Mechanical characterisation of the TorPeDO: A low frequency gravitational force sensor," Classical Quantum Gravity 34, 135002 (2017).
- 30D. Fiorucci, J. Harms, M. Barsuglia et al., "Impact of infrasound atmospheric noise on gravity detectors used for astrophysical and geophysical applications," Phys. Rev. D 97, 062003 (2018).
- ³¹Streckheisen GmbH, STS-2 Broadband Sensor-Manual (1995); available at https://www.passcal.nmt.edu/webfm_send/488

- ³²M. P. Ross, T. Mistry, L. Datrier et al., "Initial results from the LIGO Newtonian calibrator," Phys. Rev. D 104, 082006 (2021).
- ⁵³L. Matone, P. Raffai, S. Márka et al., "Benefits of artificially generated gravity gradients for interferometric gravitational-wave detectors," Classical Quantum Gravity 24, 2217 (2007).
- 34C. Hagedorn and J. G. Lee, NEWT (Newtonian Eot-Wash Toolkit) (2021); available at https://github.com/4kbt/NewtonianEotWashToolkit
- 35N. A. Holland et al., "Measured characterization of the torsion pendulum dual oscillator controls prototype," (2023) (unpublished).
- 36P. W. F. Forsyth, "Simulation and isolation design for the TorPeDO gravitational sensor," Ph.D. thesis (The Australian National University, 2022).
- ³⁷J. V. van Heijningen, A. Bertolini, E. Hennes et al., "A multistage vibration isolation system for advanced Virgo suspended optical benches," Classical Quantum Gravity 36, 075007 (2019).
- ⁵⁸Nanometrics, Inc., Trillium: Broadband seismometer—Specification Sheet (2005); available at https://www.passcal.nmt.edu/webfm_send/1467
- 39 A. Kulur Ramamohan *et al.*, "Characterization of heterodyne phase locking for a Newtonian noise sensor," (2023) (unpublished).